



Impacts of stronger winds and less sea ice on Canadian Beaufort Sea shelf ecosystems since the late 1990s

Jade Falardeau^{a,*}, Anne de Vernal^a, Bianca Fréchette^a, Claude Hillaire-Marcel^a, Philippe Archambault^b, Michael Fritz^c, Colin P. Gallagher^d, George Tanski^c

^a Geotop Research Center in Earth System Dynamics, Département des sciences de la Terre et de l'atmosphère, Université du Québec à Montréal, C.P. 8888 Succursale Centre-Ville, H3C 3P8, Montréal, Canada

^b Takuvik, ArcticNet, Québec Océan, Département de biologie, Université Laval, 1045 avenue de la Médecine, G1V 0A6, Québec, Canada

^c Permafrost Research Unit, Alfred Wegener Institute, Helmholtz Centre for Polar and Marine Research, Telegrafenberg A45, 14473, Potsdam, Germany

^d Fisheries and Oceans Canada, Arctic and Aquatic Research Division, Freshwater Institute, 501 University Crescent, Winnipeg, Manitoba, R3T-2N6, Canada

ARTICLE INFO

Keywords:

Sea ice
Coastal erosion
Salinity
Permafrost
Benthic foraminifera
Tintinnids
Ostracods
Micropaleontology
Arctic ocean

ABSTRACT

Continuous and multi-decadal records of faunal abundance and diversity helping to identify the impacts of ongoing global warming on aquatic ecosystems are rare in the coastal Arctic. Here, we used a 50-year-long microfaunal record from a sediment core collected in the Herschel Basin (YC18-HB-GC01; 18 m water depth) to document some aspects of the environmental responses of the southern Canadian coastal Beaufort Sea to climate change. The microfaunal indicators include benthic foraminiferal assemblages, ostracods and tintinnids. The carbonate shells of two foraminiferal species were also analyzed for their stable isotope signatures ($\delta^{13}\text{C}$ and $\delta^{18}\text{O}$). We compiled environmental parameters from 1970 to 2019 for the coastal region, including sea ice data (break-up date, freeze-up date, open season length and mean summer concentration), the wind regime (mean speed, direction of strong winds and the number of storms), hydrological data (freshet date, freshet discharge and mean summer discharge of the Firth and the Mackenzie rivers), and air temperature. Large-scale atmospheric patterns were also taken into consideration. Time-constrained hierarchical clustering analysis of foraminiferal assemblages and environmental parameters revealed a near-synchronous shift around the late 1990s. The microfaunal shift corresponds to an increased abundance of taxa tolerant to variable salinity, turbulent bottom water conditions, and turbid waters towards the present. The same time interval is marked by stronger easterly winds, more frequent storms, reduced sea-ice cover, and a pervasive anticyclonic circulation in the Arctic Ocean (positive Arctic Ocean Oscillation; AOO+). Deeper vertical mixing in the water column in response to intensified winds was fostered by increased open surface waters in summer leading to turbulence, increased particle loading and less saline bottom waters at the study site. Stronger easterly winds probably also resulted in enhanced resuspension events and coastal erosion in addition to a westward spreading of the Mackenzie River plume, altogether contributing to high particulate-matter transport. Increase food availability since ~2000 was probably linked to enhanced degradation of terrestrial organic carbon, which also implies higher oxygen consumption. The sensitivity of microfaunal communities to environmental variations allowed capturing consequences of climate change on a marine Arctic shelf ecosystem over the last 50 years.

1. Introduction

Severe environmental changes in the coastal habitats of the south-eastern Beaufort Sea due to global warming include sea-ice loss (Frey et al., 2015), increased coastal erosion rates (Irrgang et al., 2018), and the Mackenzie River plume spreading into open waters (Mulligan and Perrie, 2019). These modifications of the nearshore habitat can affect

the distribution, quality, and diversity of marine resources (e.g., Brewster et al., 2016; Gallagher et al., 2021), with consequences on food security, culture, and economy of northern communities that rely on marine ecosystem for subsistence (Fritz et al., 2017). Identifying relationships between biota and their habitat can help local stakeholders to find adaptation strategies to climate change. However, studies that combine faunal and climatic records are sparse, and the existing records

* Corresponding author. Geotop-UQAM, C.P. 8888 Succursale Centre-Ville, H3C 3P8, Montréal, Canada.

E-mail address: Falardeau.jade@courrier.uqam.ca (J. Falardeau).

<https://doi.org/10.1016/j.ecss.2023.108520>

Received 21 April 2023; Received in revised form 21 August 2023; Accepted 1 October 2023

Available online 13 October 2023

0272-7714/© 2023 Elsevier Ltd. All rights reserved.

often cover too short or discontinuous observational periods, which makes it difficult to disentangle the impacts of recent anthropogenic climate warming versus natural climate and environmental variability. Paleoceanographic reconstructions with high temporal resolution can help fill the gap (e.g., Lapointe et al., 2017; Nguyen et al., 2017; Kutos et al., 2021; Gemery et al., 2023).

Microorganisms of Arctic Ocean shelves have been widely used as indicators of marine conditions. Their distribution is related to water temperature, salinity, oxygen levels, contaminants, and surface productivity (Cearreta et al., 2000; Wollenburg and Kuhnt, 2000; Polyak et al., 2002; Stepanova et al., 2003; Ruiz et al., 2005 and references therein; Gemery et al., 2017). In sediment archives, these microorganisms can be used to develop time series, providing that sedimentary processes are favorable to continuous and fine particle accumulation, which is uncommon in dynamic nearshore areas.

In this study, we established an ecological record spanning the last 50 years based on the analyses of microfaunal community changes in the Herschel Basin on the Beaufort Sea continental shelf, Canada. In addition to microfaunal assemblages, we analyzed the isotopic composition of the carbonate shells of two benthic foraminiferal species to further document bottom water conditions. In parallel, we compiled instrumental and satellite data of different environmental parameters including sea-ice, wind, hydrography, air temperature, and large-scale atmospheric pattern. By comparing both datasets, we seek to investigate potential relationships between ecological and environmental changes and to identify potential stressors in a rapidly evolving Arctic nearshore zone. This study also aims to validate the use of micropaleontological tools to reconstruct the impacts of recent climate changes on Arctic coastal areas, where in-situ measurements and ecosystem-based monitoring programs are limited (cf. Fritz et al., 2017; Brewster et al.,

2021).

2. Study area

The Canadian Beaufort Sea continental shelf is ~530 km long and up to ~120 km wide. It is flanked by the Mackenzie Delta to the east and Herschel Island – Qikiqtaruk to the west (Fig. 1). East of the island, the Herschel Basin is 15 km wide, 40 km long, and has a maximum depth of 70 m (Fig. 1, EBA Engineering Consultants Ltd, 1992). As a natural sedimentary depocenter, it allows for a continuous accumulation of sediment and biological remains (Grotheer et al., 2020; Falardeau et al., 2023a). The shallow (<20 m) part of the continental shelf is covered by persistent land-fast ice that forms in October and lasts until late June (Carmack and Macdonald, 2002). In summer, sea-ice meltwater and river discharge generate a stratified surface water layer of 7–15 m-thick (Carmack and Macdonald, 2002; Falardeau et al., 2023a).

Predominant wind directions are an important component of the physical coastal environment. Under strong easterly winds, sea ice is pushed offshore, nutrient-rich subsurface waters upwell (Carmack and Macdonald, 2002; Pickart et al., 2011), and the Mackenzie River plume spread up to hundreds of kilometers westward (Mulligan and Perrie, 2019). Inversely, strong westerly winds tend to maintain sea ice and the river plume close to shore.

The Mackenzie River is among the four largest rivers discharging into the Arctic Ocean with an annual mean flux of $316 \text{ km}^3 \cdot \text{a}^{-1}$ (for 1999–2008; Holmes et al., 2012). The Mackenzie River plume, particularly during the spring freshet, brings fresh and particle-rich waters onto the shelf (Ehn et al., 2019). Two smaller rivers close to the study site, the Firth and Babbage rivers (Fig. 1), and smaller river systems, also contribute to freshwater with dissolved- and particulate-matter input (e.

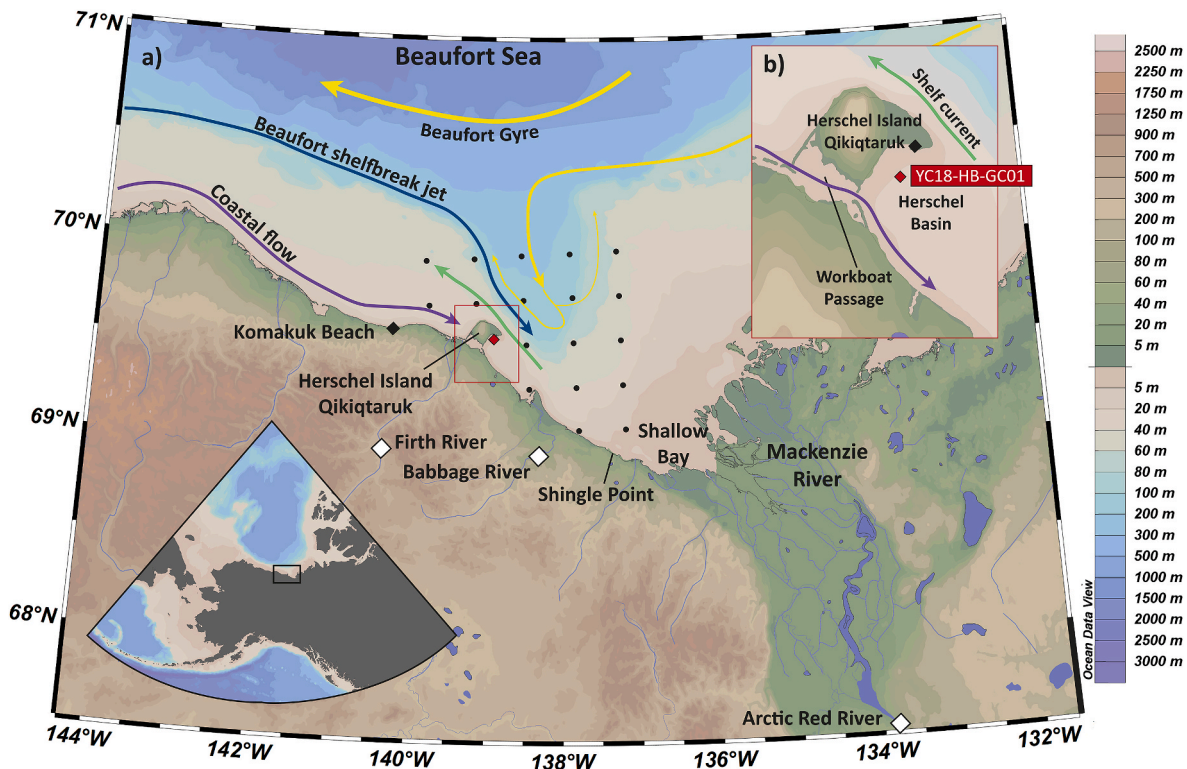


Fig. 1. a) Study area in the southern Canadian Beaufort Sea and b) close-up of the core site location. White and black diamonds represent the location of the hydrometric and weather stations, respectively. The black dots correspond to the grid used to calculate the mean summer sea-ice concentration. The purple arrow corresponds to the longshore current carrying low saline waters derived from the coastal river outflows and the extension of the Alaskan coastal waters; the blue arrow corresponds to the nutrient-rich and saline (>31.5) Pacific waters flowing through the “Beaufort Sea shelfbreak jet” (Pickart, 2004); the yellow arrows show the Beaufort Gyre and the associated recirculation currents and finally, the green arrow identified in (b) indicates the cold (<-1 °C) and low salinity (<31) surface waters (<30 m) flowing through the shelf current (Lin et al., 2020). Maps were made in Ocean Data View (Schlitzer, 2018). (For interpretation of the references to colour in this figure legend, the reader is referred to the Web version of this article.)

g., Coch et al., 2018).

3. Material and methods

3.1. Microfaunal analyses

Remains of microorganisms were analyzed in the sediment core YC18-HB-GC-01 (Fig. 1; 69.544°N-138.970°W; 18 m water depth; hereafter HBGC01) collected in the Herschel Basin in August 2018. The coring site is located approximately 4 km east of the Herschel Island coast and 125 km west of the Mackenzie River mouth at Shallow Bay (Fig. 1). The core was retrieved with a UWITEC gravity corer from a Zodiac inflatable boat and stored at +4 °C until further analyses. The HBGC01 core was cut in halves lengthwise and subsampled at 1-cm intervals for micropaleontological and radio-isotope analyses. The 40 cm-long core spanned from ~1970 to 2018 with a mean sediment accumulation rate of $0.9 \pm 0.3 \text{ g cm}^{-2} \text{ a}^{-1}$ allowing for a near-annual resolution (Falardeau et al., 2023a; Fig. A1d). The age model was built based on ^{210}Pb radiogenic activities and sediment density using the *Plum* package (Aquino-López et al., 2018) in R (R Core Team, 2021). Sediment laminations and a mixed ^{210}Pb excess signal in the core top 10 cm suggested reworking (Hill and Nadeau, 1989; Fig. A1a, c). However, the ^{210}Pb log-decrease between the bottom of the core and 10 cm led to estimating a mean sedimentation rate of $0.8 \text{ cm} \cdot \text{a}^{-1}$, which was fed into the *Plum* age model. An independent ^{137}Cs peak at 38-37 cm suggested an age of 1963 (Aoyama et al., 2006) that roughly matched the age interval of 1963–1981 given by the age model (Fig. A1d; see Falardeau et al., 2023a for more details).

For microfossil counts, 6–7 g of dry sediment per sample were wet-sieved at 63 µm and the upper fraction was observed under a stereo microscope at a magnification of 40 to 60X. The samples contain three main types of microfossils: benthic foraminifera (calcareous and agglutinated, inclusively), ostracods, and tintinnids. Foraminifera were identified according to Feyling-Hanssen et al. (1971), Polyak et al. (2002), and Scott et al. (2008), while ostracods identification was based on Stepanova et al. (2003) and Gemery et al. (2017). The only species of tintinnid observed in the dried fraction >63 µm is *Tintinnopsis fimbriata* (Meunier, 1919), which is an agglutinated ciliate that inhabits the upper 40 m of the water column (Paranjape, 1987). For this study, the abundance of microfossils is expressed in fluxes ($\# \cdot \text{cm}^{-2} \cdot \text{a}^{-1}$), which is the number of specimens counted per gram of sediment in one sample ($\# \cdot \text{g}^{-1}$) multiplied by the accumulation rates ($\text{g} \cdot \text{cm}^{-2} \cdot \text{a}^{-1}$). For more details on microfossil preparations, species identification, and microfaunal diversity in the Herschel Basin see Falardeau et al. (2023a).

We analyzed the assemblages of the benthic foraminifera and reported the relative abundance of species in percentages (%; calcareous and agglutinated foraminifera together). For the purpose of this paper, only the relative abundances of the taxa with clear ecological affinities are discussed (see Table 1).

3.2. Geochemistry

3.2.1. Carbonate shells

The carbonate shells of the two most abundant calcareous benthic foraminiferal species, *Elphidium clavatum* and *Cassidulina reniforme*, were analyzed for their stable isotopic composition ($\delta^{18}\text{O}$ and $\delta^{13}\text{C}$, ‰ vs. VPDB) at the light stable isotope geochemistry laboratory of Geotop-UQAM following standard laboratory procedures. Briefly, the specimens from the >63 µm fraction of each species were weighed using a microbalance, which yielded between 50 and 120 µg of material per sample. The weighed specimens were subsequently transferred into conical glass vials, closed with septum caps, and heated at 90° for an hour before the analysis, which is performed using a Micromass Iso-prime isotope ratio mass spectrometer coupled to a MultiCarb system in dual inlet mode. The results are normalized based on two internal references (UQ6: $\delta^{18}\text{O} = -1.48 \pm 0.03\text{‰}$ and $-14.25 \pm 0.05\text{‰}$; NBS18:

Table 1

List of the microfaunal taxa, the corresponding abbreviation names, and their ecological affinities when applicable. *Selected ecological indicators used in this study (see Fig. 2a).

Abbreviation	Species	Ecological affinities	Reference
B. frig	<i>Buccella frigida</i>	Tolerant to low salinity in Arctic shelves	Polyak et al. (2002); Scott et al. (2008); Wollenburg and Kuhnt (2000)
C. ren	<i>Cassidulina reniforme</i>	Stable saline bottom waters	Polyak et al. (2002); Scott et al. (2008)
E. alb	<i>Elphidium albiumbilicatum</i>		
E. ask	<i>Elphidium asklundi</i>	Tolerant to low salinity	Falardeau et al. (2023a)
E. bart	* <i>Elphidium bartletti</i>	Varying and generally low salinities; Coarse-grained substrate	Polyak et al. (2002); Falardeau et al. (2023a)
E. clav	<i>Elphidium clavatum</i>		
E. pul	* <i>Eoepionidella pulchella</i>	Food availability and upwelling	Wollenburg and Kuhnt (2000); Scott et al. (2008); Falardeau et al. (2023a)
E. tak	<i>Epistominella takayanagii</i>		
H. orb	<i>Haynesina orbicularis</i>	Tolerant to low salinity in Arctic shelves	Polyak et al. (2002); Scott et al. (2008)
H. niv	* <i>Haynesina nivea</i>	Shallow environments; Fresh, warm and unstable water conditions	Voltski et al. (2015); Falardeau et al. (2023a)
I. hel	<i>Islandiella helena</i>	Cold and relatively low salinity waters in shallow Arctic shelves; Near sea-ice margins	Cage et al. (2021)
I. nor	* <i>Islandiella norcrossi</i>	Stable saline waters	Polyak et al. (2002); Cage et al. (2021)
Poly	Polymorphinids		
Q. stalk	* <i>Quinqueloculina stalker</i>	Associated to glacier-proximal facies; Tolerate turbidity; Can feed on bacterial degradation products	Guilbault et al. (2003); Falardeau et al. (2023b)
R. turb	<i>Recurvoides turbinatus</i>		
S. fey	* <i>Stainforthia feytingi</i>	Sea-ice margin productivity	Seidenkrantz (2013)
S. bif	<i>Spiroplectammina biformis</i>	Rapid sedimentation and turbid meltwaters	Jennings and Helgadóttir (1994)
S. hor	* <i>Stetsonia horvathi</i>	Oligotrophic waters under permanently ice-covered regions; Can feed on bacterial degradation products	Wollenburg and Kuhnt (2000); Jennings et al. (2020); Falardeau et al. (2023b)
T. ear	* <i>Textularia earlandi</i>	Opportunistic; Can feed on bacterial degradation products; Tolerate turbidity	Alve (2010); Jennings et al. (2020); Falardeau et al. (2023b)
T. tor	<i>Textularia torquata</i> <i>Tintinnopsis fimbriata</i>	Fresh sediment-loaded waters; Near river mouths	Echols and Fowler (1973); Falardeau et al. (2023a)

$\delta^{13}\text{C} = 2.21 \pm 0.03\text{‰}$ and $-40.78 \pm 0.05\text{‰}$; see raw data in Table A1).

3.2.2. Bulk sediment

Geochemical analyses on the bulk sediments of core HBGC01

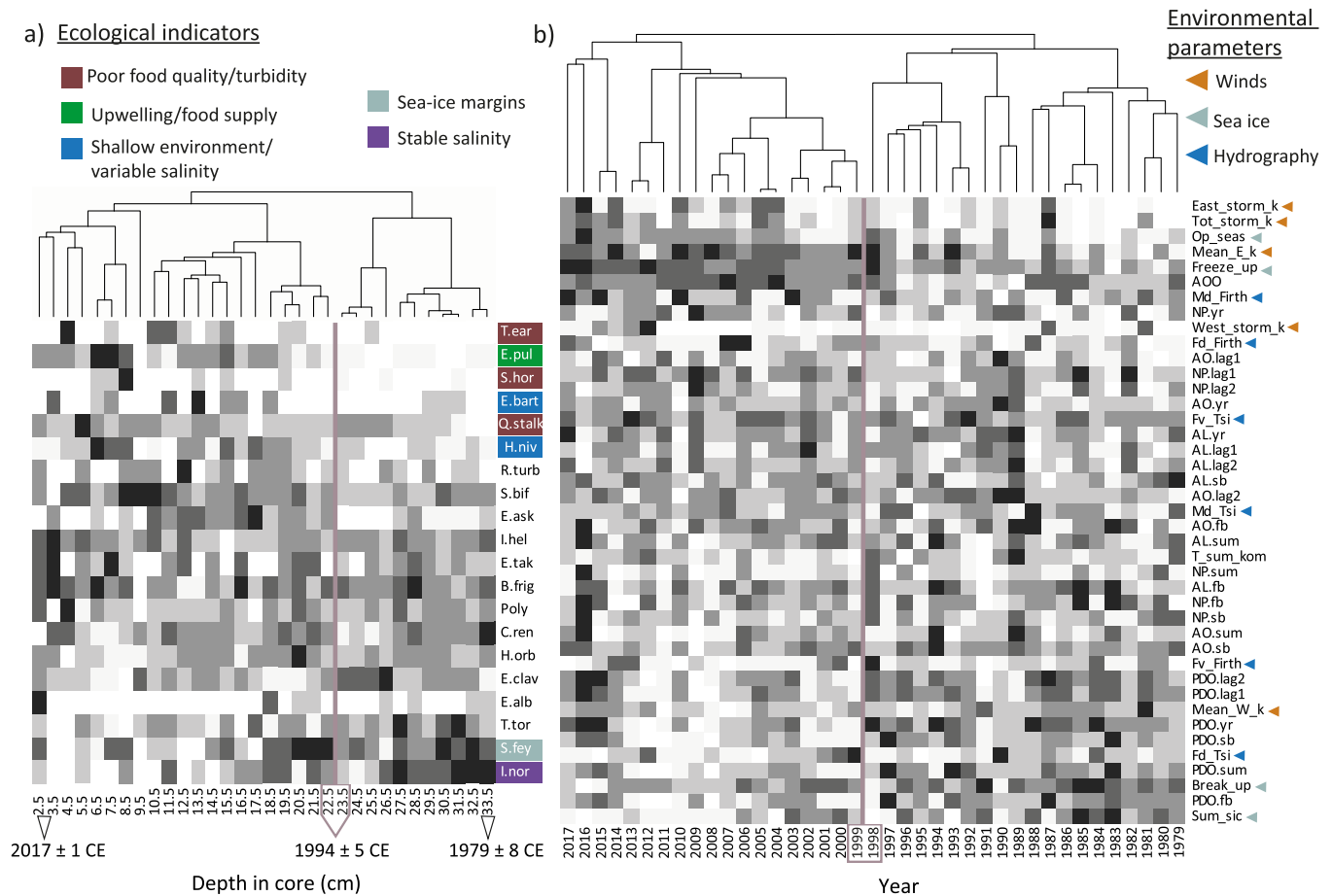


Fig. 2. Heat maps and time-constrained hierarchical clusters illustrated as dendrograms of the (a) foraminiferal relative abundances, including the selected ecological indicators, and the (b) environmental parameters reordered based on their weighted average from the cluster score. See [Tables 1 and 2](#) for the ecological affinity references and the abbreviation corresponding names.

comprise the total organic carbon (TOC) and the total nitrogen (TN) together with the stable isotopic ratios of organic carbon ($\delta^{13}C_{org}$) and nitrogen ($\delta^{15}N$). For each subsample, about 1 g of homogenized freeze-dried sediment was weighed at UQAM before being sent to the Stable Isotope Facility of the University of California (Davis, USA). Following their procedures, the inorganic carbon and moisture of ~5–30 mg of subsamples were removed by fumigation with hydrochloric acid (37%) for 72 h and by treatment with NaOH pellets for 1–2 days, respectively, both at a temperature of 60 °C. The TOC and TN were measured with an ECS 4010 Elemental Analyzer (Costech) and are given in weight percent (wt %). The $\delta^{13}C$ and $\delta^{15}N$ were measured using an Elementar Vario El Cube elemental analyzer coupled to an Isoprime VisION IRMS (Elementar) or a PDZ Europa 20-20 isotope ratio mass spectrometer (Sercon). The results are reported per mil relative to the Vienna Pee Dee Belemnite (‰ vs. VPDB) or the air standards (‰ vs. N air) for carbon and nitrogen, respectively. The atomic C/N ratio was obtained by multiplying the TOC/TN ratio with the atomic mass ratio of N/C (i.e. 14/12; see raw data in [Table A2](#)).

3.3. Environmental parameters

3.3.1. Sea-ice cover and seasonality

To quantify the daily sea-ice concentrations in the study area (area covered by sea ice in %), the mean of 18 grid points (25 km × 25 km) was calculated from the NOAA/NSIDC climate data record of passive microwave sea-ice concentration covering the 1979–2018 interval (data from [Meier et al., 2017](#); see [Fig. 1](#) for grid point locations). The metrics include the mean summer (June, July, August, and September; JJAS)

sea-ice concentration followed by the break-up and freeze-up dates defined as 10 consecutive days with less than 50% and over 50% of sea-ice concentration, respectively, from which the length of the ice-free season was obtained.

3.3.2. Wind data

We used the hourly wind data from the Komakuk Beach weather station ([Fig. 1](#); [Environment and Climate Change Canada Historical Climate Data, 2020b](#)), which covers from 1973 to 2018. Measurements were made every 6 h from 1973 to 1993, and every hour, from 1994 to 2018. Gaps that were smaller than 6 consecutive hours were interpolated from linear regression. The interpolated hourly 1994–2018 record was then subsampled every 6 h to avoid an overrepresentation of the data in this interval. Only the hourly wind data within the open water season were considered for all calculated wind indices.

We analyzed the direction of winds $>10 \text{ m s}^{-1}$, which exhibited a clear bimodal pattern ([Fig. A2](#)) as winds originated either from the east or the west (east: 45°–135° and west: 225°–315°). We calculated the mean wind speed per open water season for both directions. We also calculated the annual frequency of storm events, which are described as six consecutive hours with winds $>10 \text{ m s}^{-1}$ (cf. [Manson and Solomon, 2007](#)). A storm event was thus recorded when two consecutive readings $>10 \text{ m s}^{-1}$ occurred. Data from the Herschel Island weather station are also available ([Fig. 1b](#)), but the temporal coverage is too short and discontinuous for being included in this study (see [Fig. A2](#) and [Table A3](#)).

Table 2

List of the environmental parameters and their corresponding abbreviation names.

T_sum_kom	Mean summer air temperature at Komakuk Beach (°C)
Fd_Tsi	Freshet date at Arctic Red River (Julian Day)
Md_Tsi	Mean summer discharge at Arctic Red River (m ³ ·s ⁻¹)
Fv_Tsi	Freshet discharge value at Arctic Red River (m ³ ·s ⁻¹)
Fd_Firth	Freshet date at Firth River (Julian Day)
Md_Firth	Mean summer discharge at Firth River (m ³ ·s ⁻¹)
Fv_Firth	Freshet discharge value at Firth River (m ³ ·s ⁻¹)
sum_sic	Mean summer sea-ice concentration (%)
break_up	Date of sea-ice break-up (Julian Day)
Op_seas	Number of ice-free days
Freeze_up	Date of sea-ice freeze-up (Julian Day)
mean_E_k	Mean easterly wind speed during the open water season at Komakuk Beach (m·s ⁻¹)
mean_W_k	Mean westerly wind speed during the open water season at Komakuk Beach (m·s ⁻¹)
east_storm_k	Number of easterly storms at Komakuk Beach
west_storm_k	Number of westerly storms at Komakuk Beach
tot_storm_k	Total number of storms at Komakuk Beach
NP	North Pacific Index
PDO	Pacific Decadal Oscillation
AOO	Arctic Ocean Oscillation
AO	Arctic Oscillation
AL	Aleutian Low-Beaufort Sea Anticyclone (ALBSA)
yr	Mean of the twelve months prior to the open water season (i.e., June)
sum	Summer mean (JJAS)
sb	Spring bloom (JJ) mean
fb	Fall bloom (AS) mean
lag1	Mean of the three months (MAM) before the open water season
lag2	Mean of the six months (DJFMAM) before the open water season

3.3.3. River discharge

Time-series of daily discharge data were retrieved online from the Firth River Near the Mouth, the Babbage River Below Caribou Creek, and the Mackenzie River at the Arctic Red River hydrometric stations (Fig. 1; Environment and Climate Change Canada Historical Hydro-metric Data, 2020). Discharge data cover 46 years (1972–2018), 18 years (1978–1994), and 44 years (1973–2017), respectively. Three hydrometric indices are used to describe the river dynamics: (1) the spring freshet date, (2) the freshet discharge, and (3) the mean summer discharge (July, August, and September; JAS), after the spring freshet date. The spring freshet date was defined as the day of the highest discharge between May and June. Due to its short temporal coverage, the Babbage River will not be discussed any further (see data in Fig. A3 and Table A3).

3.3.4. Air temperatures

Air temperature data were obtained from the Environment and Climate Change Canada Historical Climate Data (2020a). The mean summer (JJAS) air temperature was calculated based on the daily mean air temperatures at Komakuk Beach (1958–2017) and at Herschel Island (1995–2018) weather stations (Fig. 1; Table A3), but only the longer record of Komakuk Beach was used for further analyses.

3.3.5. Atmospheric oscillation indices

We acquired the monthly means of different atmospheric oscillation indices including the North Pacific Index (NPI; Trenberth and Hurrell, 1994), the Aleutian Low-Beaufort Sea Anticyclone (ALBSA; Cox et al., 2019), the Arctic Oscillation (AO; Thompson and Wallace, 1998) and the Pacific Decadal Oscillation (PDO; Mantua et al., 1997) from the NOAA Physical Sciences Laboratory website (<https://psl.noaa.gov/>). Subsequently, we calculated the summer (JJAS) mean for these indices, in addition to the spring bloom (June and July) and the fall bloom (August and September) means. To evaluate if there was a level of predictability of the climate indices on the following summer environmental conditions, we also calculated the mean of the indices for the three months (March, April, and May; MAM), the six months (December to May;

DJFMAM) and the twelve months before the beginning of the summer season (June). Finally, the annual Arctic Ocean Oscillation index (AOO; Proshutinsky and Johnson, 1997; <https://www.who.edu/page.do?pid=66578>) was also used in this study. A summary of the atmospheric oscillation indices used in this study and their potential linkages with the southern Beaufort Sea environmental conditions are presented in Table A4.

3.4. Cluster analyses and rate of change

The continuous temporal coverage between the ecological indicators and the environmental parameters spans from 1979 to 2017. Data from the sediment core were treated independently because of uncertainties with regard to the age model and the irregular time steps between the sediment subsamples. To identify discontinuities in the time-series and to keep the chronological order, we used a time-constrained hierarchical cluster analysis. For the foraminiferal assemblages, we applied the *Bray-Curtis* dissimilarity on the square-root transformed foraminiferal relative abundances, i.e. the *Hellinger* transformed foraminiferal raw counts. The square-root transformation reduces the importance of the abundant taxa, and inversely, gives more importance to the lower-numbered taxa. Only the species recording >1% in at least one sample were kept for statistical analyses (n = 20 taxa; Fig. 2a). For the environmental dataset that includes parameters of different units and scales, the cluster was applied on the *Euclidean* distance of the z-scores transformed parameters (n = 41 parameters; Fig. 2b). We used the constrained hierarchical clustering function (*chclust*) of the *rioja* package (Juggins, 2022) in R (R Core Team, 2021). Subsequently, the relative abundances of the taxa were normalized on a scale of 0–5 and ordered based on their weighted average from the cluster score using the *vegemite* function of the *vegan* package in R (Oksanen et al., 2013) and illustrated with a heat map (Fig. 2a). The same approach was used for the environmental parameters (Fig. 2b). Only the variables that demonstrated ruptures or changes within the covered time interval are discussed in this study.

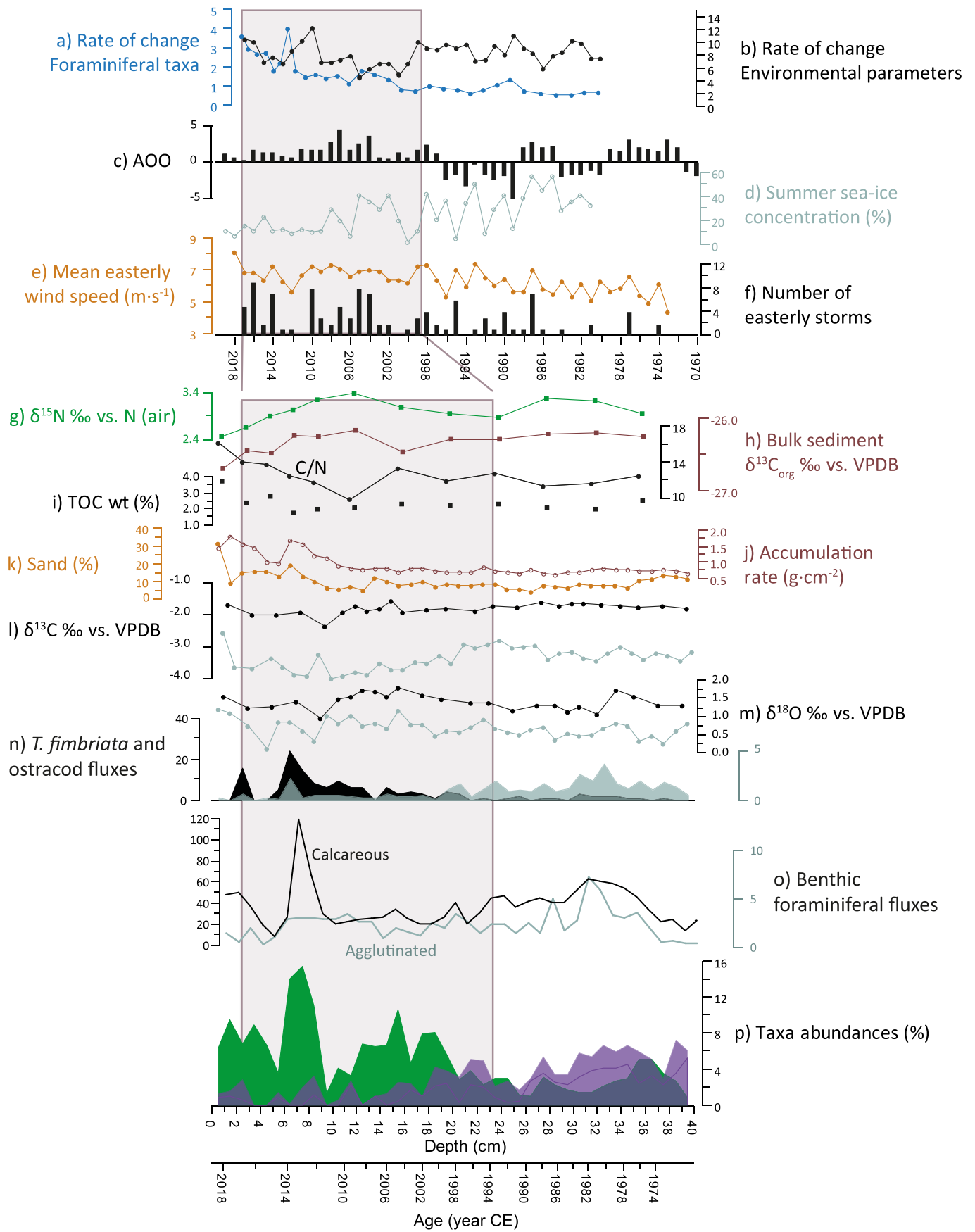
We also calculated an index of the rate of change per year for the foraminiferal and environmental data, which corresponds to the *Bray-Curtis* dissimilarity or the *Euclidean* distance for the foraminiferal assemblages and the environmental data, respectively, between adjacent samples or years in both chronosequences. The distance calculation was applied to the square-root transformed foraminiferal relative abundances and the z-score transformed environmental parameters. To obtain a rate of change per year, the *Euclidean* distance of the foraminiferal assemblages was divided by the elapsed time between samples. All the environmental data are available in Table A3.

4. Results and discussion

4.1. Environmental changes

The dendrogram of the time-constrained hierarchical clustering of the environmental parameters places the first division in 1998–1999 (Fig. 2b). The two resultant subsets are mainly determined by the intensification of easterly storms and the total number of storms (Fig. 2b and 3f). Accordingly, the mean easterly wind speed increases towards the present and frequently reach values above 6 m s⁻¹ (Fig. 3e). Other important changes recorded around 1998 involve sea ice conditions (Fig. 2b). While the break-up occurred on average 18 days earlier in 1998–2017, the average freeze-up date was delayed by 15 days, implying an increased open water season of about one month (Table A3). This trend is reflected in the summer sea-ice concentration, which decreased from 34 ± 14% before 1998 to 18 ± 11% afterwards (Fig. 3d).

The hydrographical indicators do not particularly stand out in the analysis, except for a possible increase in the Firth River mean summer discharge and an earlier freshet of the Mackenzie River towards the present (Figs. 2b, A3). The summer mean discharge of the Firth River



(caption on next page)

Fig. 3. Summary figure of regional changes from the 1970s to 2018 as recorded in the study core, and the environmental and climatic archives. Rate of change of the a) benthic foraminiferal assemblages and the b) environmental parameters (see section 3.4). c), d), e), and f) Selected environmental indicators. g), h) and i) Geochemical measurements performed in the HBGC01 core together with the atomic C/N ratio (black line). j) Accumulation rates ($\text{g}\cdot\text{cm}^{-2}$) and k) concentration of sand (%). l) $\delta^{13}\text{C}$ and m) $\delta^{18}\text{O}$ of *Elphidium clavatum* (gray) and *Cassidulina reniforme* (black). n) Fluxes ($\#\cdot\text{cm}^{-2}\cdot\text{a}^{-1}$) of *Tintinnopsis fimbriata* (black shaded area) and ostracod valves (gray shaded area) and o) fluxes of calcareous (black line) and agglutinated (gray line) benthic foraminifera. p) Relative abundance (%) of *Eoepionidella pulchella* (green shaded area) and the cumulative abundance (%) and the cumulative abundance (%) of *Islandiella norcrossi* and *Stainforthia feylingi* from 1970 to 2018 (see Falardeau et al., 2023a). The solid purple line delineates the abundance of *S. feylingi* (below) and *I. norcrossi* (above). The gray shaded areas highlight the 1999–2017 and the 1994–2017 subsets of the foraminiferal taxa and the environmental parameters, respectively. (For interpretation of the references to colour in this figure legend, the reader is referred to the Web version of this article.)

increased by about $50\text{ m}^3\cdot\text{s}^{-1}$ over the 2005–2018 interval (Fig. A3). The waters of the Firth River and the organic matter they carry may reach the Herschel Basin as the currents flow dominantly from west to east through the Workboat Passage adjacent to the southern shore of Herschel Island (Fig. 1; Pelletier and Medioli, 2014). The Mackenzie River freshet occurred on average one week earlier since the beginning of the 1990s (Fig. A3). The PDO has generally been negative after 1998 (Fig. 2b) while the AOO became positive after 1997 (Figs. 2b and 3c). Lower environmental variability after 2000 is suggested by a decrease in the rate of change (Fig. 3b).

4.2. Changes in the marine habitat

4.2.1. Microfaunal community

The dendrogram of the time-constrained hierarchical clustering for the foraminiferal assemblages places the main division of the full 1979–2017 time interval at 23 cm, which corresponds to an age of 1994 ± 5 years (Fig. 2a). The 1979–1994 subgroup was marked by abundant *Islandiella norcrossi* and *Stainforthia feylingi*, which decrease afterwards as *Textularia earlandi*, *Eoepionidella pulchella*, *Elphidium bartletti*, *Quinqueloculina stalkerii*, *Stetsonia horvathi* and *Haynesina nivea* increase (Fig. 2a).

The two main subsets of foraminiferal taxa are characterized by different levels of tolerance to low salinity waters and unstable conditions. While *Islandiella norcrossi* typically prefers stable saline conditions, *Haynesina nivea* and *Elphidium bartletti* occupy shallow environments with variable temperatures and salinities, along with relatively turbulent bottom waters (Table 1). The taxon *Stainforthia feylingi* is also more abundant at a deeper site of the Herschel Basin, which suggests a preference for calm and stable environmental conditions (Falardeau et al., 2023a). The height and number of branches in the dendrogram are higher in the 1994–2017 interval than from 1979 to 1994, which illustrates that neighboring assemblages are less comparable after ~1994 (Fig. 2a). Accordingly, the trend in the rate of change continuously increases and shows repeated peaks of particularly high values after ~1998 (Fig. 3a). This behavior is coherent with more dissimilar and changing foraminiferal assemblages, thus suggesting more unstable marine coastal habitat conditions during the last two decades.

The two subsets of foraminiferal taxa may also reflect preferences for different types of food given the inverse relationship between species feeding on degradation products by bacteria (i.e. *Quinqueloculina stalkerii*, *Textularia earlandi* and *Stetsonia horvathi*) or on food associated with upwelling and primary productivity (i.e., *Eoepionidella pulchella*), and a species (i.e., *Stainforthia feylingi*) that feed near sea-ice margins (Table 1; Figs. 2a and 3p). The transition around 1994 is also marked by a decrease in ostracod fluxes from a mean of 1.5 ± 0.8 valves $\cdot\text{cm}^{-2}\cdot\text{g}^{-1}$ before repeatedly near-zero values afterwards. Inversely, the tintinnid *Tintinnopsis fimbriata* was nearly absent before ~1994, after which its flux increased, peaking at $24\text{ cm}^{-2}\cdot\text{g}^{-1}$ (Fig. 3n). The average calcareous benthic foraminiferal fluxes is lower after ~1994 (Fig. 3o, black line). However, the fluxes show large amplitude variations since ~2010 with a distinct peak in calcareous foraminiferal abundance of $119\text{ cm}^{-2}\cdot\text{g}^{-1}$ around 2014. Minimum values are recorded at the bottom and top of the core, which coincide with intervals of reduced agglutinated benthic foraminiferal fluxes (Fig. 3o).

4.2.2. Geochemistry and lithology

The $\delta^{13}\text{C}$ -values of *Elphidium clavatum* average $-3.4 \pm 0.3\text{‰}$. Negative values characterize infaunal habitat, as the interstitial water of the sediment is depleted in ^{13}C (McCorkle et al., 1997). After ~2006, the $\delta^{13}\text{C}$ -values slightly decrease reaching the lowest value of $-4.0 \pm 0.1\text{‰}$ in ~2012 (Fig. 3l, gray). The $\delta^{13}\text{C}$ -values of *Cassidulina reniforme* remain constant throughout the record ($-1.8 \pm 0.2\text{‰}$; Fig. 3l, black). The $\delta^{13}\text{C}$ of *E. clavatum* is lower than that of *C. reniforme*, suggesting that *E. clavatum* either lives at a greater depth in the sediment and/or have a faster metabolism (higher respiration rates; cf. Ravelo and Hillaire-Marcel, 2007; Cesbron et al., 2016). Decreased $\delta^{13}\text{C}$ -value in benthic foraminiferal shells can also relate to more depleted inorganic carbon in bottom waters due to high microbial respiration of organic matter (Mol et al., 2018). The $\delta^{18}\text{O}$ -values of *E. clavatum* ranged from 0.6‰ in the ~1970–2000 interval to values $> 1.0\text{‰}$ towards the core top with two relatively low values around 2012 and 2016 (Fig. 3m, gray line). *C. reniforme* also shows a trend toward higher $\delta^{18}\text{O}$ -values upcore (Fig. 3m, black line). In estuarine-like environments, increased $\delta^{18}\text{O}$ suggests increased water salinity as these variables tend to have a positive linear relationship (Polyak et al., 2003; Lansard et al., 2012).

The TOC increased from 2.2 to 3.8% towards the core top (Fig. 3i), and the $\delta^{13}\text{C}_{\text{org}}$ and $\delta^{15}\text{N}$ of bulk sediment samples decreased after ~2009 (Fig. 3g and h). The C/N ratio > 10 suggests dominant terrestrial organic matter sources, especially towards the core top (Fig. 3; cf. Magen et al., 2010; Jong et al., 2020). The changes in the grain-size distribution of the core are restricted to the last decade with sand content increasing from ~9 to 31% (Fig. 3k).

4.3. Consequences of climate change on the coastal ecosystem

4.3.1. Easterly winds, sea ice, and unstable marine conditions

Winds and sea ice-related variables recorded the most significant changes along the southeastern Beaufort Sea coast over the last five decades. The relationship between easterly winds and the reduced sea-ice cover and/or persistence is known in the region (Ogi and Wallace, 2007; Wood et al., 2013; Frey et al., 2015), as easterly winds tend to push the ice away from the shore. At the regional scale, enhanced easterly winds occur under a strong anticyclonic regime (i.e., under positive AOO; Proshutinsky and Johnson, 1997; Ogi and Wallace, 2007, Fig. 3c, d, e; Table A4). Furthermore, the potential relationship between negative PDO and reduced sea ice (Fig. 2b) in the Arctic Ocean has been documented by Screen and Francis (2016) and Lapointe et al. (2017). Hence, negative PDO normally occurs when the Aleutian Low is weak (positive NPI; Table A4), which leads to dominant southerly winds in the northern Pacific, thus to the advection of warm Pacific air towards the central Arctic. However, the effects of a negative PDO/weak Aleutian Low on the sea-ice cover of the southern Beaufort Sea is equivocal, as it also favors westerly winds (downwelling events; Kirillov et al., 2016; see section 2). Ultimately, the strength of the anticyclonic circulation in the western Arctic better accounts for wind direction and sea-ice cover changes in the area (Ogi and Wallace, 2007; Kirillov et al., 2016; this study). On land, negative PDO leads to warmer atmosphere and enhanced precipitation in the northwestern Canadian Arctic (Lapointe et al., 2017; Kutos et al., 2021), which might result in higher mean river discharge (Coch et al., 2018), and possibly earlier freshet dates (Figs. 2b, A2). The environmental parameters that stand out the most from our

cluster analysis are thus interrelated and complementary to each other (Table A4).

The environmental shift identified in 1998 is near-synchronous with the important marine habitat shift revealed by the microfaunal community in 1994 ± 5 years (Fig. 2; section 4.2.1). A reduced sea-ice cover, strong easterly winds, and the enhanced frequency of storms likely favored vertical mixing (Rainville and Woodgate, 2009; Schulze and Pickart, 2012) and a western dispersal of the Mackenzie River plume towards Herschel Island and beyond (Mulligan and Perrie, 2019). Altogether, they can account for more variability in oceanographic conditions at depth in the Herschel Basin (section 4.2.1), in accordance with the foraminiferal rate of change recording the highest values (Fig. 3a). Interestingly, lower environmental variability was recorded after 1998 (Fig. 3b). The lower summer sea-ice concentration, thus the longer open water season, might have played an important role in coastal habitat instabilities. Although environmental variability was higher before 1998, more persistent land-fast ice probably acted as a shield from the variable climatic conditions (see Falardeau et al., 2023a).

The Mackenzie River hydrography does not seem to play an important role in the coastal area near the Herschel Basin (Fig. 2b). The influence of the plume at such a distance from the river mouth appears to be more determined by wind strength and direction and sea-ice than by freshet and summer mean discharge. However, nearby tributaries and small rivers result in freshwater and organic matter inputs that may be important locally (Fig. 2b; Coch et al., 2018).

Although most ecological indicators and environmental parameters point to enhanced freshwater in the Herschel Basin during the last two decades, higher $\delta^{18}\text{O}$ values are recorded after 2000 (Fig. 3m), which is somewhat counterintuitive (Lansard et al., 2012). The benthic $\delta^{18}\text{O}$ record could reflect a shallower halocline as recently identified in the Canada Basin (Rosenblum et al., 2022). However, during the seasonal sea-ice growth, ^{18}O -depleted brines are released and sink to the sea floor, whereas during summer, sea-ice melting releases positive $\delta^{18}\text{O}$ and low-salinity meltwater into the surface water layer (Ravelo and Hillaire-Marcel, 2007). As these processes blur the current $\delta^{18}\text{O}$ -salinity relationship, an unequivocal interpretation of the shift in $\delta^{18}\text{O}$ -values seems difficult to resolve here given the combination of changes in the sea ice regime, halocline depth, and continental runoff. Nevertheless, the negative $\delta^{18}\text{O}$ values after 2006 suggest higher variability in the parameters governing the isotopic composition of benthic foraminifera (Fig. 3m).

4.3.2. Food sources and turbidity

After 1998, strong easterly winds and more frequent storms (Fig. 3e and f) favored the mixing and upwelling of nutrient-rich subsurface Pacific waters (Pickart, 2004; Pickart et al., 2011), thus increasing the regional primary productivity (Tremblay et al., 2011). Enhanced food supply might be the reason for the increased abundance of *Eoeponidella pulchella* dated around 1994 ± 5 years (Fig. 3p; Table 1). A slight increase in $\delta^{15}\text{N}$ and $\delta^{13}\text{C}_{\text{org}}$, and a lower C/N around 2010 (Fig. 3g and h) may also indicate enhanced export of fresh marine algae (Magen et al., 2010). Alternatively, the concomitant increase of *T. fimbriata* (Fig. 3n, black shaded area), *Quinqueloculina stalkerii*, *Textularia earlandi* and *Stetsonia horvathi* abundances after ~ 1998 (Fig. 2a; Table 1) suggests that the additional supply of degraded organic matter is mainly from terrestrial sources, which can sustain nearshore marine food webs (Terhaar et al., 2021). Terrestrial organic matter could originate from the Mackenzie River plume (Magen et al., 2010) pushed by the strong easterly winds (Fig. 3e and f) or from the Firth River and other local river systems (Fig. 2b; section 4.1). It may also originate from permafrost degradation and coastal erosion (Jong et al., 2020) as sediment dispersal around Herschel Island is favored under easterly winds (Klein et al., 2019).

The intensified oxygen consumption associated with microbial degradation of organic matter (Mol et al., 2018) may explain the low

abundances of ostracods after ~ 1998 (Fig. 3n, gray shaded area) as they are sensitive to hypoxia (e.g., Ruiz et al., 2005; Stepanova et al., 2019). Moreover, *T. fimbriata* inhabits environments near river mouths (Table 1), where degradation of organic matter is important. Hence, the inverse relationship between *T. fimbriata* and ostracod abundances in the sediment (Fig. 3n) could be explained by the increased input of organic matter leading to oxygen consumption.

After 2006, when sea-ice concentration was particularly low (Fig. 3d), the increased vulnerability of cliffs and permafrost-based coastlines to wave action may have led to maximal coastal erosion rates (Overeem et al., 2011; Irrgang et al., 2018). The subsequent large supply of terrestrial matter may account for increased TOC accumulation, well-reflected in the ^{13}C -depleted TOC and the higher C/N values (Magen et al., 2010; Grotheer et al., 2020; Jong et al., 2020), and increased accumulation rates, which are all recorded in the recent years (Fig. 3h, i, j). Enhanced supply of terrestrial matter may also account for the lower $\delta^{13}\text{C}$ -values in *Elphidium clavatum* (Fig. 3l, gray), which can be indicative of enhanced respiration of ^{13}C depleted organic matter (cf. Ravelo and Hillaire-Marcel, 2007; Mol et al., 2018). Furthermore, terrestrial matter could result from the strengthened vertical mixing and bottom currents under more frequent ice-free conditions (Rainville and Woodgate, 2009) that cause the resuspension of fine particles and reworking (Hill and Nadeau, 1989; Jong et al., 2020), which is documented by the relative enrichment in sand content (Fig. 3d, k). The parallel increase of sand and TOC might illustrate alternating episodes of accumulation vs. reworking (Jong et al., 2020), which add to unstable conditions in the nearshore marine habitat. A coarser sediment substrate can also account for changes in the benthic microfaunal assemblages (Polyak et al., 2002; Gemery et al., 2021; Falardeau et al., 2023a).

While the species diversity of foraminifera did not vary significantly over the last decades, the most notable impact of the recent climate change in the benthic foraminiferal community is recorded through a change in the proportions of accompanied species (Fig. 2a; Falardeau et al., 2023a). More importantly, the rate at which the assemblages changed since the late 1990s is unprecedented over the last millennia (Falardeau et al., 2023b). Additionally, the increase in sand content, which results from intense and frequent vertical mixing due to strong winds, is associated with lower benthic foraminiferal abundances, especially the agglutinated ones (Fig. 3k, o, gray line). A dilution of the microfossil content by detrital input cannot be discarded, but should be minimized by using microfaunal fluxes. Moreover, since the preservation of the microfossils is good throughout the HBGC01 sediment core, their decreased abundance likely relates to reduced productivity of agglutinated foraminifera (Falardeau et al., 2023a).

5. Conclusions

At the onset of the 21st century, the coastal area of the southern Canadian Beaufort Sea was marked by the intensification of mean summer easterly wind speed and storm frequency accompanied by reduced summer sea-ice cover concentration and a longer open water season. Accordingly, the beginning of the 21st century also corresponds to a strong anticyclonic regime in the Arctic Ocean (AOO+), which favored easterly winds, and dominantly negative PDO, leading to reduced sea-ice cover and contributing to the advection of warm Pacific air in the western Arctic Ocean. Such environmental conditions were marked by a significant shift in the coastal benthic habitats as documented by the microfossil assemblages, geochemical tracers, and lithological indices.

After ~ 1994 , the ecological indicators suggest more turbulent bottom water conditions with enhanced freshwaters leading to variable salinities in the coastal environment, most probably related to more intensive vertical mixing of the upper freshwater layer due to longer ice-free seasons and stronger winds. This phenomenon probably intensified during the last decade when particularly low sea-ice concentration led to increased sediment reworking and resuspension. In addition, the coastal

Beaufort Sea was probably marked by an enhanced supply of terrestrial organic matter. Part of the terrestrial inputs may have been carried by the Mackenzie River plume, which also plays a role in freshwater fluxes, and from resuspension and erosion of the nearby coasts, both occurring under strong easterly winds.

The impacts of the environmental shift are mainly recorded in the proportions of many benthic foraminiferal species in the assemblages. The rapid rate at which these assemblages changed, unprecedented on the time scale of centuries, emphasizes the importance to continue the monitoring of the benthic microfauna in the forthcoming years. Moreover, increased terrestrial input probably led to enhanced microbial degradation of organic matter. This process contributes to oxygen consumption, which may have negatively affected animals such as ostracods, and extend to other benthic organisms. Furthermore, the organic matter is mainly transported within particulate-rich waters. High turbidity can affect light penetration and raises concerns about the potential of primary producers to achieve photosynthetic activity, with consequences for primary consumers and higher trophic levels of the marine food web.

CRediT authorship contribution statement

Jade Falardeau: Writing – original draft, Visualization, Project administration, Investigation, Funding acquisition, Formal analysis, Conceptualization. **Anne de Vernal:** Writing – review & editing, Supervision, Funding acquisition, Conceptualization. **Bianca Fréchette:** Writing – review & editing, Formal analysis. **Claude Hillaire-Marcel:** Writing – review & editing. **Philippe Archambault:** Writing – review & editing, Supervision, Conceptualization. **Michael Fritz:** Writing – review & editing, Supervision, Resources, Funding acquisition, Conceptualization. **Colin P. Gallagher:** Writing – review & editing, Conceptualization. **George Tanski:** Writing – review & editing, Resources.

Declaration of competing interest

The authors declare that they have no known competing financial interests or personal relationships that could have appeared to influence the work reported in this paper.

Data availability

Data used in this study are in the supplementary tables or already published in Falardeau et al. (2023)

Acknowledgment

This study was possible thanks to the Fonds de Recherche du Québec Nature et Technologies (FRQNT) for their financial support to JF through scholarships and to the Geotop Research Center. We also thank the Natural Sciences and Engineering Research Council (NSERC) who provided funds to AdV through a Discovery and a CREATE grant [432295; ArcTrain]. We acknowledge the Northern Scientific Training Program of Polar Knowledge Canada and the EU Horizon 2020 project Nunataryuk [grant no. 773421] for making the fieldwork on Herschel Island – Qikiqtaruk Territorial Park and the community consultations possible. In particular, we thank Chief Ranger Richard Gordon and his team. We thank Konstantin Klein and Léo Chassiot, who helped in the field. We wish to thank our colleagues who contributed to this study: Charles Brunette for sea-ice data, Pascal Bourgault for historical climate and hydrometric data extraction, Hussein Wazneh for his help in R coding, and Paul Myers for his advice on atmospheric oscillation indices. We finally wish to acknowledge the reviewers who helped in improving our manuscript and who provided us with insightful comments.

Appendix A. Supplementary data

Supplementary data to this article can be found online at <https://doi.org/10.1016/j.ecss.2023.108520>.

References

- Alve, E., 2010. Benthic foraminiferal responses to absence of fresh phytodetritus: a two-year experiment. *Mar. Micropaleontol.* 76, 67–75.
- Aoyama, M., Hirose, K., Igarashi, Y., 2006. Re-construction and updating our understanding on the global weapons tests 137Cs fallout. *J. Environ. Monit.* 8, 431–438.
- Aquino-López, M.A., Blaauw, M., Christen, J.A., Sanderson, N.K., 2018. Bayesian analysis of ²¹⁰Pb dating. *J. Agric. Biol. Environ. Stat.* 23, 317–333.
- Brewster, J., Neumann, D., Ostertag, S., Loseto, L., 2016. Traditional ecological Knowledge (TEK) at shingle point, YK: observations on changes in the environment and fish populations. In: Characterizing the Diet and Habitat Niches of Coastal Fish Populations in the Beaufort Sea Tarium Niryutait Marine Protected Area 121.
- Brewster, J.D., Hansen-Craik, K., Harwood, L., Blakeston, C., 2021. State of Tarium Niryutait Marine Protected Areas (TNMPA) Report: Inventory of Monitoring from 2010-2016. Department of Fisheries and Oceans Canada.
- Cage, A.G., Pieńkowski, A.J., Jennings, A., Knudsen, K.L., Seidenkrantz, M.-S., 2021. Comparative analysis of six common foraminiferal species of the genera *Cassidulina*, *Paracassidulina*, and *Islandiella* from the Arctic–North Atlantic domain. *J. Micropalaeontol.* 40, 37–60.
- Carmack, E.C., Macdonald, R.W., 2002. Oceanography of the Canadian shelf of the Beaufort Sea: a setting for marine life. *Arctic* 29–45.
- Cearreta, A., Irabien, M.J., Leorri, E., Yusta, I., Croudace, I., Cundy, A., 2000. Recent anthropogenic impacts on the Bilbao estuary, northern Spain: geochemical and microfaunal evidence. *Estuar. Coast Shelf Sci.* 50, 571–592.
- Cesbron, F., Geslin, E., Jorissen, F., Delgard, M.-L., Charrieau, L., Deflandre, B., Jézéquel, D., Anschutz, P., Metzger, E., 2016. Vertical distribution and respiration rates of benthic foraminifera: contribution to aerobic remineralization in intertidal mudflats covered by *Zostera noltei* meadows. *Estuar. Coast Shelf Sci.* 179, 23–38.
- Coch, C., Lamoureux, S.F., Knoblauch, C., Eischeid, I., Fritz, M., Obu, J., Lantuit, H., 2018. Summer rainfall dissolved organic carbon, solute, and sediment fluxes in a small Arctic coastal catchment on Herschel Island (Yukon Territory, Canada). *Arctic Science* 4, 750–780.
- Cox, C.J., Stone, R.S., Douglas, D.C., Stanitski, D., Gallagher, M., 2019. The Aleutian Low-Beaufort Sea Anticyclone: a climate index correlated with the timing of springtime melt in the Pacific Arctic cryosphere. *Geophys. Res. Lett.* 46, 7464–7473.
- EBA Engineering Consultants Ltd, 1992. Proceedings of the Beaufort Sea Granular Resources Workshop, Part 1: Reports on NOGAP Regional Studies, p. 11.
- Echols, R.J., Fowler, G.A., 1973. Agglutinated tintinnid loricae from some Recent and Late Pleistocene shelf sediments. *Micropaleontology* 19, 431–443.
- Ehn, J.K., Reynolds, R.A., Stramski, D., Doxaran, D., Lansard, B., Babin, M., 2019. Patterns of suspended particulate matter across the continental margin in the Canadian Beaufort Sea during summer. *Biogeosciences* 16, 1583–1605.
- Environment and Climate Change Canada Historical Climate Data, 2020. Retrieved April. https://climate.weather.gc.ca/index_e.html.
- Environment and Climate Change Canada Historical Climate Data, 2020. Retrieved October. https://climate.weather.gc.ca/index_e.html.
- Environment and Climate Change Canada Historical Hydrometric Data, 2020. Retrieved April. https://wateroffice.ec.gc.ca/mainmenu/historical_data_index_e.html.
- Falardeau, J., de Vernal, A., Seidenkrantz, M.-S., Cronin, T.M., Gemery, L., Chassiot, L., Fritz, M., Carnero-Bravo, V., Hillaire-Marcel, C., Archambault, P., 2023a. Microfaunal recording of recent environmental changes in the Herschel basin, western Arctic Ocean. *J. Foraminifer. Res.* 53, 20–48.
- Falardeau, J., de Vernal, A., Seidenkrantz, M.-S., Fritz, M., Cronin, T.M., Gemery, L., Rochon, A., Carnero-Bravo, V., Hillaire-Marcel, C., Pearce, C., Archambault, P., 2023b. A 1300-year microfaunal record from the Beaufort Sea shelf indicates exceptional climate-related environmental changes over the last two centuries. *Palaeogeogr. Palaeoclimatol. Palaeoecol.* 625, 111670.
- Feyling-Hanssen, R.W., Jørgensen, J.A., Knudsen, K.L., Lykke-Andersen, A.-L., 1971. Late quaternary foraminifera from vendssyssel, Denmark and sandnes, Norway. *Geological Society of Denmark* 21, 67–317.
- Frey, K.E., Moore, G., Cooper, L.W., Grebmeier, J.M., 2015. Divergent patterns of recent sea ice cover across the bering, chukchi, and Beaufort seas of the pacific arctic region. *Prog. Oceanogr.* 136, 32–49.
- Fritz, M., Vonk, J.E., Lantuit, H., 2017. Collapsing arctic coastlines. *Nat. Clim. Change* 7, 6–7.
- Gallagher, C.P., Courtney, M.B., Seitz, A.C., Lea, E.V., Howland, K.L., 2021. Ocean-entry timing and marine habitat-use of Canadian Dolly Varden: dispersal among conservation, hydrocarbon exploration, and shipping areas in the Beaufort Sea. *Estuar. Coast Shelf Sci.* 262 <https://doi.org/10.1016/j.ecss.2021.107609>.
- Gemery, L., Cronin, T.M., Briggs, W.M., Brouwers, E.M., Schormikov, E.I., Stepanova, A., Wood, A.M., Yasuhara, M., 2017. An Arctic and Subarctic ostracode database: biogeographic and paleoceanographic applications. *Hydrobiologia* 786, 59–95.
- Gemery, L., Cronin, T.M., Cooper, L.W., Dowsett, H.J., Grebmeier, J.M., 2021. Biogeography and ecology of ostracoda in the US northern bering, chukchi, and Beaufort seas. *PLoS One* 16. <https://doi.org/10.1371/journal.pone.0251164>.
- Gemery, L., Cronin, T.M., Cooper, L.W., Roberts, L.R., Keigwin, L.D., Addison, J.A., Leng, M.J., Lin, P., Magen, C., Marot, M.E., Schwartz, V., 2023. Multi-proxy record of

- ocean-climate variability during the last two millennia on the Mackenzie Shelf, Beaufort Sea. *Micropaleontology* 69, 345–366.
- Grotheer, H., Meyer, V., Riedel, T., Pfalz, G., Mathieu, L., Hefter, J., Gentz, T., Lantuit, H., Mollenhauer, G., Fritz, M., 2020. Burial and origin of permafrost-derived carbon in the nearshore zone of the southern Canadian Beaufort Sea. *Geophys. Res. Lett.* 47 <https://doi.org/10.1029/2019GL085897>.
- Guilbault, J.-P., Barrie, J.V., Conway, K., Lapointe, M., Radi, T., 2003. Paleoenvironments of the Strait of Georgia, British Columbia during the last deglaciation: microfaunal and microfloral evidence. *Quat. Sci. Rev.* 22, 839–857.
- Hill, P.R., Nadeau, O.C., 1989. Storm-dominated sedimentation on the inner shelf of the Canadian Beaufort Sea. *J. Sediment. Res.* 59, 455–468.
- Holmes, R.M., McClelland, J.W., Peterson, B.J., Tank, S.E., Bulygina, E., Eglinton, T.I., Gordeev, V.V., Gurtovaya, T.Y., Raymond, P.A., Repeta, D.J., 2012. Seasonal and annual fluxes of nutrients and organic matter from large rivers to the Arctic Ocean and surrounding seas. *Estuar. Coast* 35, 369–382.
- Irrgang, A.M., Lantuit, H., Manson, G.K., Günther, F., Grosse, G., Overduin, P.P., 2018. Variability in rates of coastal change along the Yukon coast, 1951 to 2015. *J. Geophys. Res.: Earth Surf.* 123, 779–800.
- Jennings, A.E., Helgadóttir, G., 1994. Foraminiferal assemblages from the fjords and shelf of eastern Greenland. *J. Foraminif. Res.* 24, 123–144.
- Jennings, A., Andrews, J., Reilly, B., Walczak, M., Jakobsson, M., Mix, A., Stoner, J., Nicholls, K.W., Cheseby, M., 2020. Modern foraminiferal assemblages in northern nares strait, petermann fjord, and beneath petermann ice tongue, NW Greenland. *Arctic Antarct. Alpine Res.* 52, 491–511.
- Jong, D., Bröder, L., Tanski, G., Fritz, M., Lantuit, H., Tesi, T., Haghpor, N., Eglinton, T. I., Vonk, J.E., 2020. Nearshore zone dynamics determine pathway of organic carbon from eroding permafrost coasts. *Geophys. Res. Lett.* 47 <https://doi.org/10.1029/2020GL088561>.
- Juggins, S., 2022. Rioja: Analysis of Quaternary Science Data. R package version 1.0-5. <https://cran.r-project.org/package=rioja>.
- Kirilov, S., Dmitrenko, I., Tremblay, B., Gratton, Y., Barber, D., Rysgaard, S., 2016. Upwelling of Atlantic Water along the Canadian Beaufort Sea continental slope: favorable atmospheric conditions and seasonal and interannual variations. *J. Clim.* 29, 4509–4523.
- Klein, K.P., Lantuit, H., Heim, B., Fell, F., Doxaran, D., Irrgang, A.M., 2019. Long-term high-resolution sediment and sea surface temperature spatial patterns in Arctic nearshore waters retrieved using 30-year landsat archive imagery. *Rem. Sens.* 11 <https://doi.org/10.3390/rs11232791>.
- Kutos, O., Rochon, A., Montero-Serrano, J.C., 2021. Evolution of palaeo-sea-surface conditions and sediment dynamics over the last 2700 years on the Mackenzie Slope, Beaufort Sea (Canadian Arctic). *Boreas* 50, 893–914.
- Lansard, B., Mucci, A., Miller, L.A., Macdonald, R.W., Gratton, Y., 2012. Seasonal variability of water mass distribution in the southeastern Beaufort Sea determined by total alkalinity and $\delta^{18}\text{O}$. *J. Geophys. Res.: Oceans* 117. <https://doi.org/10.1029/2011JC007299>.
- Lapointe, F., Francus, P., Lamoureux, S.F., Vuille, M., Jenny, J.-P., Bradley, R.S., Massa, C., 2017. Influence of North Pacific decadal variability on the western Canadian Arctic over the past 7000 years. *Clim. Past* 13, 411–420.
- Lin, P., Pickart, R.S., Fissel, D., Ross, E., Kasper, J., Bahr, F., Torres, D.J., O'Brien, J., Borg, K., Melling, H., 2020. Circulation in the vicinity of Mackenzie Canyon from a year-long mooring array. *Prog. Oceanogr.* 187 <https://doi.org/10.1016/j.pocan.2020.102396>.
- Magen, C., Chaillou, G., Crowe, S.A., Mucci, A., Sundby, B., Gao, A., Makabe, R., Sasaki, H., 2010. Origin and fate of particulate organic matter in the southern Beaufort Sea–Amundsen Gulf region. *Canadian Arctic. Estuarine, Coastal and Shelf Science* 86, 31–41.
- Manson, G.K., Solomon, S.M., 2007. Past and future forcing of Beaufort Sea coastal change. *Atmos.-Ocean* 45, 107–122.
- Mantua, N.J., Hare, S.R., Zhang, Y., Wallace, J.M., Francis, R.C., 1997. A Pacific interdecadal climate oscillation with impacts on salmon production. *Bull. Am. Meteorol. Soc.* 78, 1069–1080.
- McCorkle, D.C., Corliss, B.H., Farnham, C.A., 1997. Vertical distributions and stable isotopic compositions of live (stained) benthic foraminifera from the North Carolina and California continental margins. *Deep Sea Res. Oceanogr. Res. Pap.* 44, 983–1024.
- Meier, W.N., Fetterer, F., Savoie, M., Mallory, S., Duerr, R., Stroeve, J., 2017. NOAA/NSIDC Climate Data Record of Passive Microwave Sea Ice Concentration. Version 3. [goddard_merged_seaice_conc]. NSIDC: National Snow and Ice Data Center, Boulder, Colorado USA [January 2020].
- Meunier, A., 1919. Mikroplankton de la mer Flamande. III. Les Périidiniens, vol. 8. Mémoires du Musée Royal d'Histoire Naturelle de Belgique, pp. 1–116.
- Mol, J., Thomas, H., Myers, P.G., Hu, X., Mucci, A., 2018. Inorganic carbon fluxes on the Mackenzie shelf of the Beaufort Sea. *Biogeosciences* 15, 1011–1027.
- Mulligan, R.P., Perrie, W., 2019. Circulation and structure of the Mackenzie River plume in the coastal Arctic Ocean. *Continental Shelf Res.* 177, 59–68.
- Nguyen, L., Pilfold, N.W., Derocher, A.E., Stirling, I., Bohart, A.M., Richardson, E., 2017. Ringed seal (*Pusa hispida*) tooth annuli as an index of reproduction in the Beaufort Sea. *Ecol. Indic.* 77, 286–292.
- Ogi, M., Wallace, J.M., 2007. Summer minimum Arctic sea ice extent and the associated summer atmospheric circulation. *Geophys. Res. Lett.* 34 <https://doi.org/10.1029/2007GL029897>.
- Oksanen, J., Blanchet, F.G., Kindt, R., Legendre, P., Minchin, P.R., O'Hara, R., Simpson, G.L., Solymos, P., Stevens, M.H.H., Wagner, H., 2013. Package 'vegan', Community Ecology Package, p. 295 version 2.
- Overeem, I., Anderson, R.S., Wobus, C.W., Clow, G.D., Urban, F.E., Matell, N., 2011. Sea ice loss enhances wave action at the Arctic coast. *Geophys. Res. Lett.* 38 <https://doi.org/10.1029/2011GL048681>.
- Paranjape, M.A., 1987. The seasonal cycles and vertical distribution of tintinnines in Bedford Basin, Nova Scotia, Canada. *Can. J. Zool.* 65, 41–48.
- Pelletier, B.R., Medioli, B.E., 2014. Environmental Atlas of the Beaufort Coastlands. Geological Survey of Canada.
- Pickart, R.S., 2004. Shelfbreak circulation in the alaskan Beaufort Sea: mean structure and variability. *J. Geophys. Res.: Oceans* 109. <https://doi.org/10.1029/2003JC001912>.
- Pickart, R.S., Spall, M.A., Moore, G.W., Weingartner, T.J., Woodgate, R.A., Aagaard, K., Shimada, K., 2011. Upwelling in the alaskan Beaufort Sea: atmospheric forcing and local versus non-local response. *Prog. Oceanogr.* 88, 78–100.
- Polyak, L., Korsun, S., Febo, L.A., Stanovoy, V., Khusid, T., Hald, M., Paulsen, B.E., Lubinski, D.J., 2002. Benthic foraminiferal assemblages from the southern Kara Sea, a river-influenced Arctic marine environment. *J. Foraminif. Res.* 32, 252–273.
- Polyak, L., Stanovoy, V., Lubinski, D.J., 2003. Stable isotopes in benthic foraminiferal calcite from a river-influenced Arctic marine environment. Kara and Pechora Seas: *Paleoceanography* 18. <https://doi.org/10.1029/2001PA000752>.
- Proshutinsky, A.Y., Johnson, M.A., 1997. Two circulation regimes of the wind-driven Arctic Ocean. *J. Geophys. Res.: Oceans* 102. <https://doi.org/10.1029/97JC00738>.
- R Core Team, 2021. R: A Language and Environment for Statistical Computing. R Foundation for Statistical Computing, Vienna, Austria. URL: <https://www.R-project.org/>.
- Rainville, L., Woodgate, R.A., 2009. Observations of internal wave generation in the seasonally ice-free Arctic. *Geophys. Res. Lett.* 36 <https://doi.org/10.1029/2009GL041291>.
- Ravelo, A.C., Hillaire-Marcel, C., 2007. Chapter eighteen the use of oxygen and carbon isotopes of foraminifera in paleoceanography. *Developments in marine geology* 1, 735–764.
- Rosenblum, E., Stroeve, J., Gille, S.T., Lique, C., Fajber, R., Tremblay, L.B., Galley, R., Loureiro, T., Barber, D.G., Lukovich, J.V., 2022. Freshwater input and vertical mixing in the Canada Basin's seasonal halocline: 1975 versus 2006–2012. *J. Phys. Oceanogr.* 52 <https://doi.org/10.1175/JPO-D-21-0116.1>.
- Ruiz, F., Abad, M., Bodergat, A.-M., Carbonel, P., Rodríguez-Lázaro, J., Yasuhara, M., 2005. Marine and brackish-water ostracods as sentinels of anthropogenic impacts. *Earth Sci. Res.* 72, 89–111.
- Schlitzer, R., 2018. Ocean Data View. Alfred Wegener Institute. <https://odv.awi.de>.
- Schulze, L.M., Pickart, R.S., 2012. Seasonal variation of upwelling in the Alaskan Beaufort Sea: impact of sea ice cover. *J. Geophys. Res.: Oceans* 117. <https://doi.org/10.1029/2012JC007985>.
- Scott, D.B., Schell, T., Rochon, A., Blasco, S., 2008. Modern benthic foraminifera in the surface sediments of the Beaufort shelf, slope and Mackenzie trough, Beaufort Sea, Canada: taxonomy and summary of surficial distributions. *J. Foraminif. Res.* 38, 228–250.
- Screen, J.A., Francis, J.A., 2016. Contribution of sea-ice loss to Arctic amplification is regulated by Pacific Ocean decadal variability. *Nat. Clim. Change* 6, 856–860.
- Seidenkrantz, M.-S., 2013. Benthic foraminifera as palaeo sea-ice indicators in the subarctic realm—examples from the Labrador Sea–Baffin Bay region. *Quat. Sci. Rev.* 79, 135–144.
- Stepanova, A., Taldenkova, E., Bauch, H.A., 2003. Recent ostracoda from the laptev sea (arctic siberia): species assemblages and some environmental relationships. *Mar. Micropaleontol.* 48, 23–48.
- Stepanova, A., Obrochta, S., Quintana Krupinski, N.B., Hyttinen, O., Kotilainen, A., Andrén, T., 2019. Late weichselian to holocene history of the baltic sea as reflected in ostracod assemblages. *Boreas* 48, 761–778.
- Terhaar, J., Lauerwald, R., Regnier, P., Gruber, N., Bopp, L., 2021. Around one third of current Arctic Ocean primary production sustained by rivers and coastal erosion. *Nat. Commun.* 12, 1–10.
- Thompson, D.W., Wallace, J.M., 1998. The Arctic Oscillation signature in the wintertime geopotential height and temperature fields. *Geophys. Res. Lett.* 25, 1297–1300.
- Tremblay, J.É., Bélanger, S., Barber, D., Asplin, M., Martin, J., Darnis, G., Fortier, L., Gratton, Y., Link, H., Archambault, P., 2011. Climate forcing multiplies biological productivity in the coastal Arctic Ocean. *Geophys. Res. Lett.* 38 <https://doi.org/10.1029/2011GL048825>.
- Trenberth, K.E., Hurrell, J.W., 1994. Decadal atmosphere-ocean variations in the Pacific. *Clim. Dynam.* 9, 303–319.
- Voltski, I., Korsun, S., Pillet, L., Pawlowski, J., 2015. *Protelphidium niveum* (Lafrenz, 1963) and the taxonomy of “lower” elphidiids. *J. Foraminif. Res.* 45, 250–263.
- Wollenburg, J.E., Kuhnt, W., 2000. The response of benthic foraminifera to carbon flux and primary production in the Arctic Ocean. *Mar. Micropaleontol.* 40, 189–231.
- Wood, K.R., Overland, J.E., Salo, S.A., Bond, N.A., Williams, W.J., Dong, X., 2013. Is there a “new normal” climate in the Beaufort Sea? *Polar Res.* 32 <https://doi.org/10.3402/polar.v32i0.19552>.